

Small

Bioinspired Nacre-like Alumina with a Metallic Nickel Compliant-Phase Fabricated by Spark-Plasma Sintering

--Manuscript Draft--

Manuscript Number:	smll.201900573R1
Full Title:	Bioinspired Nacre-like Alumina with a Metallic Nickel Compliant-Phase Fabricated by Spark-Plasma Sintering
Article Type:	Communication
Section/Category:	
Keywords:	spark plasma sintering; bioinspired ceramics; nacre; flexural strength; fracture toughness
Corresponding Author:	Robert O. Ritchie, MA, PhD, ScD University of California Berkeley Berkeley, CA UNITED STATES
Additional Information:	
Question	Response
Please submit a plain text version of your cover letter here.	<p>April 24, 2019</p> <p>Prof. Ana V. Almeida Editor, Small Dear Prof. Almeida:</p> <p>Re: m/s # smll.201900573: "Bioinspired nacre-like alumina with a metallic nickel compliant-phase fabricated by spark-Plasma sintering" by Amy Wat, et al.</p> <p>Thank you for your review of our paper: "Bioinspired nacre-like alumina with a metallic nickel compliant-phase fabricated by spark-plasma sintering" by Amy Wat, Claudio Ferraro, Xu Deng, Andrew Sweet, Antoni Tomsia, Eduardo Saiz and myself, which we submitted for consideration for publication in Small.</p> <p>We have revised the manuscript exactly along the lines suggested by your reviewers and have enclosed a comprehensive Response to Reviewers document which describes our revisions. These revisions are also indicted in red text in the revised manuscript itself.</p> <p>We hope that with these revisions that you will now be able for find our manuscript acceptable for publication in Small.</p> <p>The revised manuscript consists of the following components:</p> <ul style="list-style-type: none">•A Word file of the main text of the manuscript, consisting of ~2800 words (including a ~600-word Experimental section), with 51 references and 3 figures.•A Supplementary information file, comprising 420 words of text focused on further details on experimental methods, 4 additional references and 3 figures. <p>For the record, all the authors have read and concur with the contents of the revised manuscript. Moreover, they declare that they have no competing interests, financial or otherwise. As corresponding author, I take full responsibility for the re submission.</p> <p>I would be grateful if you could continue to direct all correspondence concerning this manuscript directly to my attention at roritichie@lbl.gov.</p> <p>Sincerely,</p> <p>Robert O. Ritchie H.T. & Jessie Chua Distinguished Professor of Engineering University of California, Berkeley</p>

Do you or any of your co-authors have a conflict of interest to declare?	No. The authors declare no conflict of interest.
Corresponding Author Secondary Information:	
Corresponding Author's Institution:	University of California Berkeley
Corresponding Author's Secondary Institution:	
First Author:	Robert O. Ritchie, MA, PhD, ScD
First Author Secondary Information:	
Order of Authors:	Robert O. Ritchie, MA, PhD, ScD
	Amy Wat
	Claudio Ferraro
	Xu Deng
	Andrew J. Sweet
	Antoni P. Tomsia
	Eduardo G. Saiz
Order of Authors Secondary Information:	
Abstract:	<p>Many natural materials are composites comprising hard (mineral) and soft (bio-polymer) constituents arranged into complex, multiple-scale, hierarchical architectures that result in compelling combinations of mechanical properties. As such, they present an ideal "recipe" for the development of future damage-tolerant lightweight structural materials. One notable example is mimicking the brick-and-mortar structure of nacre, which has resulted in very tough bioinspired ceramics with polymeric mortars as a compliant phase. Theoretical modeling, however, has predicted that use of metallic mortars could lead to even higher damage tolerance in these materials, although it is difficult to melt-infiltrate metals into ceramic scaffolds as they cannot readily wet ceramics. To avoid this problem, we have developed an alternative ("bottom-up") approach to synthesize "nacre-like" structural ceramics containing a small fraction of a nickel mortar. These materials were fabricated using nickel-coated alumina platelets that are aligned using slip casting and rapidly sintered using spark-plasma sintering (SPS). The dewetting of the nickel mortar during sintering was avoided by using NiO-coated as well as Ni-coated platelets. As a result, we have produced a "nacre-like" alumina ceramic which is ~2-4 times tougher than monolithic alumina at a comparable flexural strength.</p>

Bioinspired Nacre-like Alumina with a Metallic Nickel Compliant-Phase Fabricated by Spark-Plasma Sintering

Amy Wat^{1,2}, Claudio Ferraro³, Xu Deng⁴, Andrew Sweet², Antoni P. Tomsia¹,
Eduardo Saiz³ and Robert O. Ritchie^{1,2*}

1. Materials Sciences Division, Lawrence Berkeley National Laboratory, Berkeley, CA 94720, USA

2. Department of Materials Science and Engineering, University of California, Berkeley, CA 94720, USA

3. Center for Advanced Structural Ceramics, Department of Materials, Imperial College London,
London SW7 2AZ, UK

4. Institute of Fundamental and Frontier Sciences, University of Electronic Science and Technology of
China, Chengdu, China

Many natural materials present an ideal “recipe” for the development of future damage-tolerant lightweight structural materials. One notable example is the brick-and-mortar structure of nacre, found in mollusk shells, which produced high-toughness, bioinspired ceramics using polymeric mortars as a compliant phase. Theoretical modeling has predicted that use of metallic mortars could lead to even higher damage-tolerance in these materials, although it is difficult to melt-infiltrate metals into ceramic scaffolds as they cannot readily wet ceramics. To avoid this problem, we developed an alternative (“bottom-up”) approach to synthesize “nacre-like” ceramics containing a small fraction of nickel mortar. These materials were fabricated using nickel-coated alumina platelets that are aligned using slip casting and rapidly sintered using spark-plasma sintering (SPS). Dewetting of the nickel mortar during sintering was prevented by using NiO-coated as well as Ni-coated platelets. As a result, we have produced a “nacre-like”

* Corresponding author: R. O. Ritchie (email: roritche@lbl.gov)

1
2
3
4 alumina ceramic displaying a resistance-curve toughness up to $\sim 16 \text{ MPa}\cdot\text{m}^{1/2}$ with a flexural
5
6 strength of $\sim 300 \text{ MPa}$.
7
8

9
10 The remarkable damage-tolerance found in natural materials is developed through
11 functional, multi-scale architectures with structural gradients and graded interfaces.^[1-6] One
12 notable example is nacre, which comprises ceramic (mineral) platelets of polycrystalline
13 aragonite ($\sim 95\%$ by volume) bonded by biopolymers in a “brick-and-mortar” structure.^[1,3,7] The
14 mineral platelets in this structure impart high strength whereas the organic mortar acts as
15 compliant layer to create ductility by permitting platelet sliding which dissipates locally high
16 stresses. To maintain strength, such sliding is limited to a few micrometers by such mechanisms
17 as frictional resistance from the surface roughness of the platelets,^[8] the tensile/shear resistance
18 of the biopolymer interphase^[9], the presence of pre-existing interlayer bridges,^[10,11] and in certain
19 species the dovetail geometry of the platelets^[12]. Toughening is generated extrinsically,^[13]
20 primarily by crack bridging leading to brick pull-out and crack-path deflection,^[14] to an extent
21 that the fracture toughness of nacre (in energy terms) is several thousand times higher than that
22 of its constituents.
23
24
25
26
27
28
29
30
31
32
33
34
35
36
37
38
39
40
41
42

43 There has been great interest in mimicking this nacre-like structure to generate high-
44 toughness ceramics. Processing techniques such as freeze-casting (ice templating),^[15-23] layer-by-
45 layer alignment,^[24,25] thermal spray processing,^[26] sedimentation,^[27] coextrusion,^[28,29] magnetic
46 platelet alignment and vacuum filtration assisted alignment^[24,30] have been used to recreate
47 brick-and-mortar microstructures. Using polymeric mortars, the nacre-like ceramics avoid
48 sudden catastrophic failure by stabilizing slow crack growth in the form of crack-resistance (R-
49 curve) behavior, although they cannot be used at elevated temperatures due to the presence of
50
51
52
53
54
55
56
57
58
59
60
61
62
63
64
65

1
2
3
4 polymer phase.^[20,24–27,31,32] Theoretical micro-mechanical modeling^[33] of synthetic “brick-and-
5
6 mortar” materials has indicated that metallic mortars may permit higher-temperature operation
7
8 while further enhancing the strength and toughness properties due to their higher shear/tensile
9
10 strength (provided the mortar strength does not exceed the brick strength).^[34] However, to
11
12 realize the full effect of a metallic mortar, the bonding between the mortar and the bricks must
13
14 be strong enough so that the vital inter-brick displacements are *within* the mortar, and not along
15
16 the brick-mortar interfaces. Moreover, processing such hybrid ceramics with a metallic
17
18 compliant phase is difficult as metals do not generally wet ceramics and thus cannot be readily
19
20 melt-infiltrated into a (*e.g.*, freeze-cast) ceramic scaffold.^[35–37]

21
22 To avoid this issue, in this study we have developed a “bottom-up approach” to create fine-
23
24 scale, high volume fraction (~95%) alumina brick-and-mortar structures with a ~5% nickel
25
26 (mortar) compliant-phase in the true image of nacre. We achieved this by coating high aspect
27
28 ratio, 0.5 to 1 μm -thick, alumina platelets (comparable in size to the mineral platelets in natural
29
30 nacre) with nickel oxide or nickel,^[38] which were then aligned using slip casting prior to spark-
31
32 plasma sintering (SPS) at 1100°C or 1200°C, as summarized in [Figure 1a](#). Details of the processing
33
34 are given in the Experimental section.

35
36 Nickel is an ideal metallic mortar because of its high melting point, strength, and ductility,
37
38 but for it to function as a reliable compliant-phase surrounding the alumina bricks in the final
39
40 nacre-like structure, it must not completely dewet from the ceramic. To achieve this, we used
41
42 both nickel- and nickel oxide-coated platelets (the coating procedures are described in [Figure S1](#)
43
44 in the Supplementary Information). Accordingly, two batches of materials were cast: one made
45
46 solely with Ni-coated platelets, the other with a mixture of NiO-coated and Ni-coated platelets.
47
48
49
50
51
52
53
54
55
56
57
58
59
60
61
62
63
64
65

1
2
3
4 By examining their fracture surfaces (Figure S2), it was apparent that slip casting had
5
6 successfully aligned the Ni+NiO-coated alumina platelets, and SPS at 1100°C and 1200°C had
7
8 completely sintered the materials into a micron-scale brick-and-mortar structure with a low
9
10 nickel content of ~5 wt.% (below 1100°C, the samples did not fully sinter). Note that SPS was not
11
12 used to sinter the ceramic platelets *per se* but rather to sinter the Ni or NiO coatings on the
13
14 platelets without dewetting in order to create samples with individual alumina “bricks” held
15
16 together by consolidated nickel “mortar” to properly replicate the toughening mechanisms
17
18 observed in its natural counterpart. The role of nickel oxide coatings was critical in limiting the
19
20 extent of dewetting by the nickel phase during sintering because controlled increases in oxygen
21
22 concentration can decrease the wetting angle without any reaction at the interface, despite a
23
24 heavily reducing graphite environment under vacuum.^[35] Specifically, the addition of oxygen
25
26 lowers the surface energy of Ni and its contact angle with alumina, which reduces the interfacial
27
28 energy between alumina and nickel and possibly the surface energy of alumina itself.^[35,39] This
29
30 reduction in surface energy is caused by adsorption or excess oxygen in the different interfaces
31
32 (the surface of Ni and the Ni-Al₂O₃ interface)^[40]. Materials sintered at 1100°C from Ni+NiO-
33
34 coated platelets did show limited signs of nickel dewetting (Figure 1b). However, those sintered
35
36 at 1100°C from solely Ni-coated platelets (Figure 1d), and at ≥1200°C for both Ni+NiO-coated
37
38 and Ni-coated platelets (Figure 1c,e), were subject to extensive dewetting, with small
39
40 agglomerates of nickel forming between the alumina platelets (sintering at >1200°C additionally
41
42 resulted in alumina grain growth). The Ni-samples sintered at 1100°C and 1200°C displayed
43
44 limited sintering between platelets as the alumina brick dimensions were $0.52 \pm 0.15 \times 6.6 \pm 2.1$
45
46 μm and are $0.54 \pm 0.15 \times 5.1 \pm 1.2 \mu\text{m}$, respectively. The Ni+NiO-samples also displayed limited
47
48
49
50
51
52
53
54
55
56
57
58
59
60
61
62
63
64
65

1
2
3
4 sintering between platelets at 1100°C and 1200°C, with alumina brick dimensions were $0.88 \pm$
5
6 $0.35 \times 6.1 \pm 1.8 \mu\text{m}$ and $1.6 \pm 0.5 \times 6.7 \pm 2.4 \mu\text{m}$, respectively. Energy-dispersive x-ray
7
8 spectroscopy of these surfaces (Figure 1b,c) confirmed the larger aggregations of nickel in
9
10 samples sintered at 1200°C, compared to the sheets of nickel when sintered at 1100°C. This
11
12 became very pronounced when the Ni+NiO-alumina samples were sintered at 1300°C (Figure
13
14
15 S3a).
16
17
18
19

20 The mechanical properties of the compliant-phase Ni-alumina and Ni+NiO-alumina
21
22 ceramics, sintered at 1100°C and 1200°C, were evaluated with respect to their flexural strength
23
24 and fracture toughness and compared with the corresponding properties of fine-grained
25
26 monolithic alumina. The flexural strength of alumina can vary between 267 and 358 MPa due to
27
28 variations in grain size or sample size.^[41] The flexural strength of our materials was comparable
29
30 to this (Figure 2a); the mean strength of our Ni+NiO-alumina sintered at 1100°C was 297.1 ± 43.1
31
32 MPa (some samples displayed strengths as high as ~350 MPa), whereas the corresponding
33
34 strength of our Ni+NiO-alumina sintered at 1200°C was ~17% lower at 246.5 ± 30.4 MPa. When
35
36 extensive dewetting of nickel occurred, as in the Ni-alumina sintered at 1100°C and 1200°C
37
38 (Figure 1d,e), the metal-ceramic interfaces are weakened from Ni dewetting such that the mean
39
40 flexural strengths decreased several-fold to $\sim 85 \pm 9.15$ MPa and $\sim 118 \pm 19.3$ MPa, respectively.
41
42
43
44
45
46
47

48 Whereas the strength does not vary much between monolithic alumina and our
49
50 (appropriately sintered) compliant-phase aluminas, the fracture toughness shows stark
51
52 differences. All the Ni-alumina samples fractured catastrophically at a particularly low
53
54 toughness without any evidence of stable crack growth, *i.e.*, no R-curve behavior (Figure 2b).
55
56 Specifically, Ni-coated samples sintered at 1100°C and 1200°C, again where extensive Ni
57
58
59
60
61
62
63
64
65

1
2
3
4 dewetting was observed (Figure 1d,e), had average fracture toughness values of 1.20 ± 0.05
5
6
7 MPa·m^½ and 2.55 ± 0.21 MPa·m^½, respectively. These values are even less than those reported
8
9
10 for monolithic alumina.^[42-44]

11
12 Clearly, the most critical aspect of processing the compliant-phase aluminas here to attain
13
14 damage-tolerant is to minimize the dewetting of the Ni mortar. As noted above, we can achieve
15
16 this through the use of 1100°C-sintered NiO-coated alumina platelets as this dramatically
17
18 increases the fracture toughness. Instead of fracturing catastrophically, the Ni+NiO-coated
19
20 alumina sintered at 1100°C displays stable crack-growth behavior, as indicated by the rising R-
21
22 curve behavior in Figure 2b, which doubles the toughness from ~7.8 MPa·m^½ at crack initiation
23
24 to 15.9 MPa·m^½ after ~250 μm of slow crack growth. Such R-curve behavior represents a six-fold
25
26 increase in fracture toughness compared to samples sintered at 1200°C, which suffer sudden
27
28 catastrophic fracture at 2.48 ± 1.10 MPa·m^½ with no evidence of rising R-curve behavior. Indeed,
29
30 the compliant-phase Ni+NiO-coated alumina sintered at 1100°C is ~2-4 times tougher than
31
32 monolithic alumina (at a comparable flexural strength).

33
34 The other key to successful processing of this high-toughness Ni+NiO-coated alumina is
35
36 spark-plasma sintering; by applying high pressures and rapid heating rates (exceeding
37
38 300°C/min, compared to conventional heating at typically ~20°C/min), **with the goal of sintering**
39
40 **only the nickel coating of the alumina platelets together while** grain growth and sintering of
41
42 alumina is **suppressed** to maintain the desired high aspect ratio of the ceramic platelets.^[45,46]
43
44 Scanning electron (SEM) micrographs of the fracture surfaces in Figure 1c show that the nickel
45
46 in the Ni+NiO-alumina samples showed only limited dewetting when sintered at 1100°C.
47
48 Indeed, the stretched and torn pieces of nickel shown in Figure 2c,d imply that the inter-brick
49
50
51
52
53
54
55
56
57
58
59
60
61
62
63
64
65

1
2
3
4 displacements, and hence the fracture path in these materials, occurred *within* the nickel mortar
5
6 layers, which is significant for obtaining optimal toughness. This was the result of the rapid
7
8 sintering with SPS, the pressure aiding flow of melted nickel, and wetting from increased oxygen
9
10 content from the NiO coatings.
11
12
13

14
15 Sintering at, or above, 1200°C was clearly detrimental because the Ni dewets excessively
16
17 forming balls of metal, despite the addition of NiO-coated platelets. A contributing factor here
18
19 is the highly reducing SPS atmosphere which can deplete oxygen in the system at higher
20
21 temperatures, making it difficult to prevent nickel dewetting. Essentially, the platelets sinter
22
23 together to form a material that is best described as alumina with a long-grained microstructure
24
25 and nickel-based inclusions. As such, the nickel no longer functions as a compliant-phase and
26
27 introduces defects into the alumina, leading to strengths and toughnesses that are lower than
28
29 monolithic alumina.
30
31
32
33

34
35 In contrast, the Ni+NiO alumina materials, spark-plasma sintered at 1100°C, displayed no
36
37 marked change in the size/shape of the ceramic bricks (at widths of $0.882 \pm 0.345 \mu\text{m}$ and lengths
38
39 of $6.06 \pm 1.8 \mu\text{m}$) with a distributed nickel phase along the ceramic-brick interfaces. This allows
40
41 for limited inter-brick displacements – the key mechanistic feature for toughness in nacre-like
42
43 materials – through the plasticity of the mortar phase. The role of the NiO coating is crucial here.
44
45 Although SPS is powerful due to its rapid sintering capabilities and continuous applied
46
47 pressure, the nickel can dewet when cooling at the end of the sintering process. The “sheet” of
48
49 Ni between the bricks was only possible due to the addition of NiO-coated alumina platelets,
50
51 which prevents the dewetting of nickel. As a result, we attained fully dense samples with a
52
53 coating of nickel acting as the mortar between the bricks. By allowing the material to display
54
55
56
57
58
59
60
61
62
63
64
65

1
2
3
4 brick pull-out, mortar phase tearing, crack bridging and deflection, as observed in nacre (Figure
5
6
7 3b,c), SPS processing at 1100°C with NiO-coated platelets generates an impressive ceramic with
8
9 a flexural strength on the order of monolithic (untoughened) alumina but with a toughness some
10
11
12 2 to 4 times higher.
13

14
15 While a marked improvement in the toughness of alumina has been achieved without loss
16
17 in strength, micromechanical modeling^[33] suggests that the damage-tolerance of these nacre-like
18
19 ceramics materials may be further improved. As noted above, the evidence in Figure 2c,d
20
21 suggests that the inter-brick displacements in the Ni+NiO alumina occur within the metallic
22
23 mortar phase rather than along the brick/mortar interfaces, but this may not be always the case.
24
25 Since the nickel layers are very thin and at times discontinuous (Figure S3b), the nickel may not
26
27 act as a completely effective “lubricating” layer between the platelets. This issue still remains the
28
29 “Achilles heel” of brick-and-mortar ceramic structures; obtaining an effective metallic mortar
30
31 with strong bonding to the ceramic bricks has yet to be completely realized. Without further
32
33 study to produce an effective mortar between the platelets, the potential for high temperature
34
35 applications for these materials have not been fully achieved. This remains the grand challenge
36
37 in the development of new bioinspired lightweight structural materials in the image of natural
38
39 nacre.
40
41
42
43
44
45
46
47

48
49 Nevertheless, the results of this work illustrate the criticality of controlling metal wetting to
50
51 create damage-tolerant ceramics with a metallic phase, *e.g.*, through the use here of NiO- as well
52
53 as Ni-coated alumina with rapid 1100°C SPS sintering. The mechanical properties of our
54
55 Ni+NiO-alumina ceramics have high damage-tolerance relative to other bioinspired ceramics
56
57 with a <10 vol.% metallic phase (Figure 3a). For example, a similar approach was used in a
58
59
60
61

1
2
3
4 previous study^[47], but the reported toughness values were an order of magnitude lower than the
5
6 ceramics developed here, which may have originated from poor bonding between the ceramic
7
8 and metallic phases (NiO-coatings were not employed). Slip-casting or freeze-casting has also
9
10 been used to process alumina/copper^[48] and alumina/nickel materials,^[47,49] and freeze-casting has
11
12 been employed to align Ni-coated alumina platelets prior to hot pressing,^[49] but in all these cases
13
14 the resulting toughnesses were significantly lower than the materials developed here, we
15
16 presume due to extensive dewetting of the metallic phase. The work of Garnier and Dunand^[49]
17
18 is notable for its use of freeze-casting to make nickel-alumina composites but these did not
19
20 replicate the structure and key mechanistic features of nacre due to their high (~30 wt.%)
21
22 nickel content, large nickel agglomerates (with diameters up to 6 μm) and consequent restricted
23
24 brick sliding which compromises toughness. Coextrusion has also been used to create nacre-like
25
26 structures with high volume fractions of ceramic and a metallic mortar, but these structures tend
27
28 to be far coarser, with brick thicknesses of hundreds of micrometers; this results in good
29
30 toughnesses up to $\sim 11 \text{ MPa}\cdot\text{m}^{1/2}$, but very low flexural strengths of 110-160 MPa.^[28,29]
31
32

33
34
35
36
37
38
39
40
41 Indeed, we believe that our Ni+NiO-alumina is the first nacre-like ceramic with a metallic
42
43 mortar displaying a flexural strength comparable to monolithic alumina ($\sim 300 \text{ MPa}$) but with a
44
45 several-fold increase in fracture toughness up to $\sim 16 \text{ MPa}\cdot\text{m}^{1/2}$ (associated with rising R-curve
46
47 behavior), a material made possible by controlling the wetting of Ni using rapid spark-plasma
48
49 sintering of slip-casting of NiO-coated and Ni-coated alumina platelets at the appropriate
50
51 temperature. The authors speculate that the limited dewetting was feasible at lower
52
53 temperatures because slower diffusion and incomplete reduction of NiO leads to more oxygen
54
55 activity at the interface between the Ni and alumina to form a lower contact angle. The limited
56
57
58
59
60
61
62
63
64
65

1
2
3
4 dewetting of the nickel mortar phase and stronger bonding between the metallic mortar and the
5
6
7 ceramic bricks are critical for imparting high strength and fracture toughness within bioinspired
8
9
10 ceramics because with ensure that the crucial inter-brick displacements and energy dispersion
11
12 at stress concentrators occur *within* the mortar. These components have generally been
13
14
15 overlooked in the scientific community's past efforts to mimic the remarkable combinations of
16
17
18 strength and fracture toughness found in natural materials.
19
20

21 **Experimental Section**

22
23
24 The starting material in the form of 0.5 -1 μm thick, 5-7 μm wide alumina platelets (Alusion®,
25
26 Antaria Limited, Australia) were coated with a nickel or nickel oxide shell using a coating
27
28 procedure modified from Shen, *et al.*^[38]. Further details are given in the Supporting Information
29
30 and are illustrated in [Figure S1](#). Slip casting of slurries was then employed, with ~50 wt.% solid
31
32 loading, to align the platelets in order to produce green bodies with a high packing density. To
33
34
35 learn how to control the nickel wetting behavior on the ceramic platelets, slurries with two
36
37
38 different compositions were prepared for sintering: one with only Ni-coated platelets and
39
40
41 another with a mixture of 20 wt.% NiO- and 80 wt.% Ni-coated alumina platelets. The
42
43
44 suspensions, which contained 10 vol.% polyvinyl alcohol (PVA) 22000 (VWR, Belgium) and 4
45
46
47 vol.% Dolapix CA (Zschimmer & Schwarz, Germany) to aid with green body strength and
48
49
50 dispersion, were manually stirred and degassed *in vacuo*. The suspensions were mixed with 63
51
52
53 vol.% water using a Thinky ARE-250 planetary mixer for 2 mins at 2,000 revolutions/min and
54
55
56 800 rotations/min with 2-min degassing between mixing steps. The slurries were poured into a
57
58
59 mold to settle, dried at 37°C for 24 hr, and baked at 100°C for 48 hr. The polymer binder in the
60
61
62
63
64
65

1
2
3
4 pellets was burnt out in argon at 500°C for 1 hr at 1°C/min in a graphite furnace (FCT Systeme,
5
6 Effelder-Rauenstein, Germany). The materials were sintered using an SPS furnace (HPD 25/1
7
8 furnace, FCT Systeme, Germany). They were compressed under vacuum at 55 MPa and heated
9
10 to 1100°C and 1200°C for 10 mins between two graphite punches inside a 20-mm diameter,
11
12 cylindrical graphite die, before slowly cooling to room temperature. Densities were measured
13
14 using the Archimedes method. A cross-section of the aligned alumina platelets after uniaxial
15
16 pressing is shown in [Figure S1](#).
17
18
19
20
21

22
23 To prepare for microstructural characterization and mechanical testing, the sintered samples
24
25 were cut perpendicular to the aligned direction with a diamond-coated saw and carefully
26
27 polished using diamond grinding discs with a final polish at 0.5 µm. The resulting 12-mm long
28
29 beams for flexural strength and fracture toughness testing had a square cross section of ~2.5 x
30
31 2.5 mm with a length of 12 mm, in general accordance with the respective ASTM D790^[50] and
32
33 ASTM E1820^[51] Standards. Flexural strength was measured on three unnotched samples for each
34
35 processing condition in three-point bending (with a loading support span of 10 mm) on an
36
37 Instron 5944 electro-mechanical testing system (Instron Corporation, Norwood, MA) at a
38
39 displacement rate of 1 µm/sec.
40
41
42
43
44
45

46
47 Corresponding fracture toughness measurements were conducted on three single edged-
48
49 notched bend SEN(B) samples for each processing condition. The notches were made using a
50
51 low-speed diamond saw and sharpened by polishing the root with a razor blade immersed in a
52
53 6-µm diamond slurry under a steady load. The resulting root radii of the notches averaged
54
55 between 6 and 20 µm. The samples were tested with an *in situ* Deben MicroTest 2kN (Deben,
56
57 UK) three-point bending apparatus with a 10 mm loading span at a displacement rate of 0.55
58
59
60
61
62
63
64
65

1
2
3
4 $\mu\text{m}/\text{sec}$ mounted inside a Hitachi S-4300SE/N (Pleasanton, CA) scanning electron microscope
5
6
7 (SEM) measure the crack-initiation fracture toughness and any subsequent subcritical crack
8
9 growth, *i.e.*, the crack resistance or R-curve, while simultaneously measuring the crack path and
10
11 imaging in real time the interaction of this path with the microstructural features. Since these
12
13 materials display some inelasticity, nonlinear-elastic fracture mechanics measurements were
14
15 used to find J -based crack resistance curves, where J is the J -integral, which describes the local
16
17 nonlinear-elastic stress at the crack tip of a nonlinear material. The standard mode I J - K
18
19 equivalence was used to find the equivalent stress-intensity values for each data point. Further
20
21 details for the calculations are also described in the Supporting Information.
22
23
24
25
26
27
28

29 **Acknowledgments**

30
31 This work was supported by the Mechanical Behavior of Materials Program (KC 13) at the
32
33 Lawrence Berkeley National Laboratory, funded by the U. S. Department of Energy, Office of
34
35 Science, Office of Basic Energy Sciences, Materials Sciences and Engineering Division, under
36
37 Contract no. DE-AC02-05CH11231. A.W. was supported by an individual National Science
38
39 Foundation Graduate Research Fellowship (Grant no. DGE 1106400). The authors would like to
40
41 acknowledge Dr. Hao Bai, Dr. Benjamin Delattre, Yuyi Li, Bryanna Benicia, Brad Takasuka, and
42
43 James Wu for their help with the experiments, and Dr. Ryan Wilkerson for his thoughtful
44
45 discussion of the work.
46
47

48 **Conflict of Interest**

49
50 The authors declare no conflict of interest.
51
52
53

54 **Keywords**

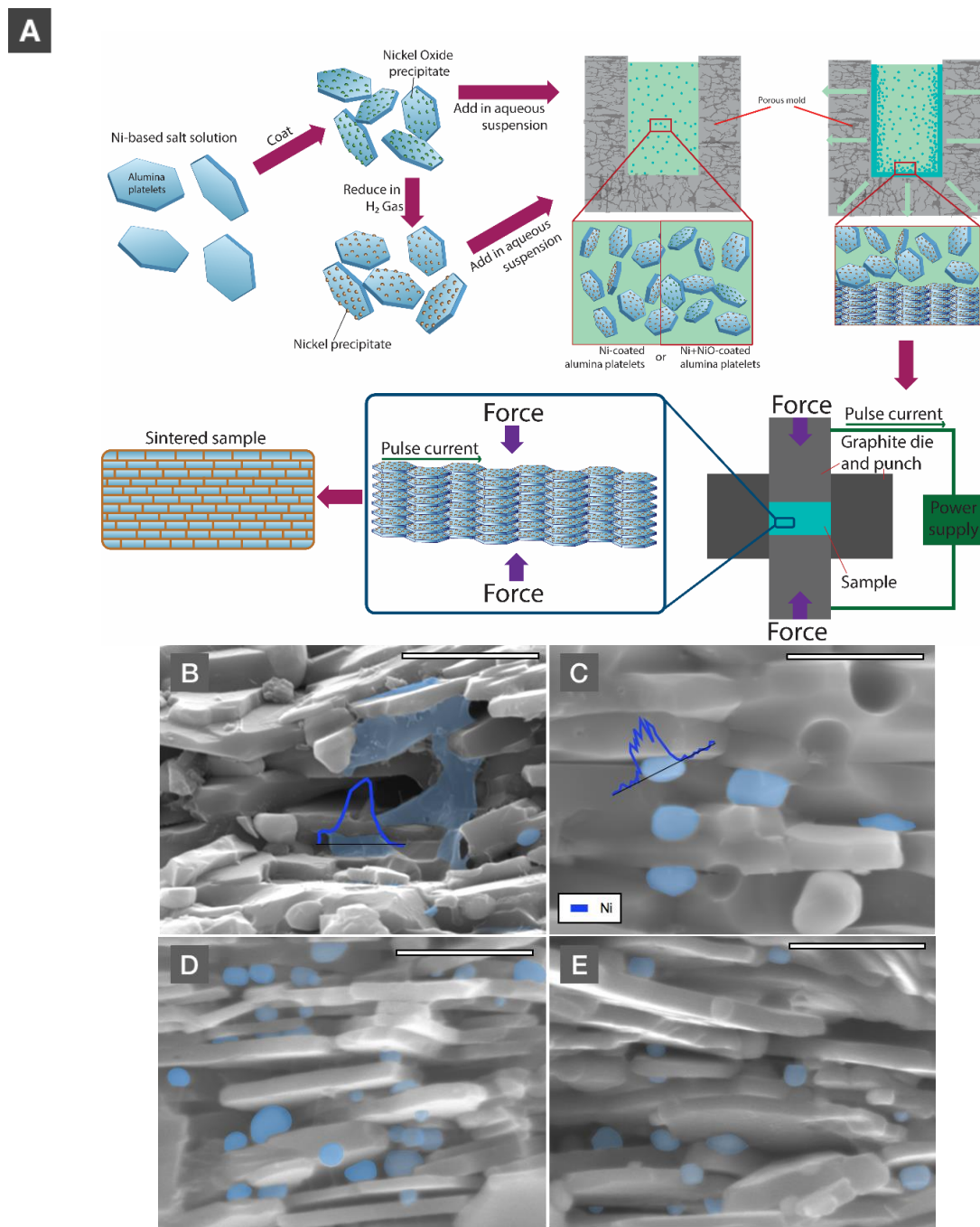
55
56 spark plasma sintering, compliant-phase ceramics, bioinspired ceramics, nacre, ceramic-metal
57
58 composites, flexural strength, fracture toughness
59
60
61

References

- [1] U. G. K. Wegst, H. Bai, E. Saiz, A. P. Tomsia, R. O. Ritchie, *Nature Mater.* **2015**, *14*, 23.
- [2] Z. Liu, M. A. Meyers, Z. Zhang, R. O. Ritchie, *Progr. Mater. Sci.* **2017**, *88*, 467.
- [3] M. A. Meyers, P.-Y. Chen, A. Y.-M. Lin, Y. Seki, *Progr. Mater. Sci.* **2008**, *53*, 1.
- [4] Y. A. Shin, S. Yin, X. Li, S. Lee, S. Moon, J. Jeong, M. Kwon, S. J. Yoo, Y.-M. Kim, T. Zhang, H. Gao, S. H. Oh, *Nature Comm.* **2016**, *7*, 10772.
- [5] S. E. Naleway, M. M. Porter, J. McKittrick, M. A. Meyers, *Adv. Mater.* **2015**, *27*, 5455.
- [6] F. Barthelat, Z. Yin, M. J. Buehler, *Nature Reviews Mater.* **2016**, *1*, 16007.
- [7] M. Sarikaya, K. E. Gunnison, M. Yasrebi, I. A. Aksay, in: P.C. Reieke, P.D. Calvert, M. Alper (eds) *Materials synthesis utilizing biological processes*: MRS Proc. vol 174. Materials Research Society, Pittsburgh, pp 109–116, 1990.
- [8] A. G. Evans, Z. Suo, R. Z. Wang, I. A. Aksay, M. Y. He, J. W. Hutchinson, *J. Mater. Res.* **2001**, *16*, 2475.
- [9] B. L. Smith, T. E. Schäffer, M. Viani, J. B. Thompson, N. A. Frederick, J. Kindt, A. Belcher, G. D. Stucky, D. E. Morse, P. K. Hansma, *Nature* **1999**, *399*, 761.
- [10] F. Song, A. K. Soh, Y. L. Bai, *Biomaterials* **2003**, *24*, 3623.
- [11] G. X. Gu, F. Libonati, S. D. Wettermark, M. J. Buehler, *J. Mech. Behav. Biomed. Mater.* **2017**, *76*, 135.
- [12] F. Barthelat, H. Tang, P. Zavattieri, C. Li, H. Espinosa, *J. Mech. Phys. Sol.* **2007**, *55*, 306.
- [13] Fracture resistance can be considered as a mutual competition between two classes of toughening mechanisms: intrinsic mechanisms, which resist microstructural damage ahead of the crack tip and are motivated primarily by plasticity, and extrinsic mechanisms, which operate at, or in the wake of, the crack tip to inhibit fracture by “shielding” the crack from the applied driving force. Whereas intrinsic toughening mechanisms are effective in inhibiting both the initiation and growth of cracks, extrinsic toughening mechanisms, such as crack bridging and crack deflection, are only effective in inhibiting crack growth.
- [14] Y. Shao, H.-P. Zhao, X.-Q. Feng, H. Gao, *J. Mech. Phys. Sol.* **2012**, *60*, 1400.
- [15] H. Bai, A. Polini, B. Delattre, A. P. Tomsia, *Chem. Mater.* **2013**, *25*, 4551.
- [16] H. Bai, F. Walsh, B. Gludovatz, B. Delattre, C. Huang, Y. Chen, A. P. Tomsia, R. O. Ritchie, *Adv. Mater.* **2015**, *28*, 50.
- [17] Y. C. Hao Bai, *Science Adv.* **2015**, *1*, e1500849.
- [18] S. Deville, E. Saiz, R. K. Nalla, A. P. Tomsia, *Science* **2006**, *311*, 515.

- 1
2
3
4 [19] V. Naglieri, H. A. Bale, B. Gludovatz, A. P. Tomsia, R. O. Ritchie, *Acta Mater.* **2013**, *61*,
5 6948.
6
7 [20] E. Munch, M. E. Launey, D. H. Alsem, E. Saiz, a P. Tomsia, R. O. Ritchie, *Science* **2008**, *322*,
8 1516.
9
10 [21] P. M. Hunger, A. E. Donius, U. G. K. Wegst, *J. Mech. Behav. Biomed. Mater.* **2013**, *19*, 87.
11
12 [22] M. M. Porter, J. Mckittrick, M. A. Meyers, *JOM* **2013**, *65*, 720.
13
14 [23] A. Wat, J. I. Lee, C. W. Ryu, B. Gludovatz, J. Kim, A. P. Tomsia, T. Ishikawa, J. Schmitz, A.
15 Meyer, M. Alfreider, D. Kiener, E. S. Park, R. O. Ritchie, *Nature Comm.* **2019**, *10*, 961.
16
17 [24] P. Das, J.-M. Malho, K. Rahimi, F. H. Schacher, B. Wang, D. E. Demco, A. Walther, *Nature*
18 *Comm.* **2015**, *6*, 5967.
19
20 [25] F. Bouville, E. Maire, S. Meille, B. Van de Moortèle, A. J. Stevenson, S. Deville, *Nature*
21 *Mater.* **2014**, *13*, 508.
22
23 [26] G. Dwivedi, K. Flynn, M. Resnick, S. Sampath, A. Gouldstone, *Adv. Mater.* **2015**, *27*, 3073.
24
25 [27] S. Behr, U. Vainio, M. Müller, A. Schreyer, G. A. Schneider, *Scientific Reports* **2015**, *5*, 9984.
26
27 [28] R. P. Wilkerson, B. Gludovatz, J. Watts, A. P. Tomsia, G. E. Hilmas, R. O. Ritchie, *Adv.*
28 *Mater.* **2016**, *28*, 10061.
29
30 [29] R. P. Wilkerson, B. Gludovatz, J. Watts, A. P. Tomsia, G. E. Hilmas, R. O. Ritchie, *Acta*
31 *Mater.* **2018**, *148*, 147.
32
33 [30] R. Libanori, R. M. Erb, A. R. Studart, *ACS Appl. Mater. Interfaces* **2013**, *5*, 10794.
34
35 [31] L. J. Bonderer, A. R. Studart, L. J. Gauckler, *Science* **2008**, *319*, 1069.
36
37 [32] R. M. Erb, R. Libanori, N. Rothfuchs, A. R. Studart, *Science* **2012**, *335*, 199.
38
39 [33] M. R. Begley, N. R. Philips, B. G. Compton, D. V. Wilbrink, R. O. Ritchie, M. Utz, *J. Mech.*
40 *Phys. Sol.* **2012**, *60*, 1545.
41
42 [34] If the mortar strength does exceed the strength of the ceramic bricks, the bricks will simply
43 fracture; this will immediately curtail the extrinsic toughening generated by crack
44 bridging and brick pull-out, with the result that the structure will fracture catastrophically
45 with a low toughness characteristic of the monolithic ceramic.
46
47 [35] E. Saiz, R. M. Cannon, A. P. Tomsia, *Annu. Rev. Mater. Res.* **2008**, *38*, 197.
48
49 [36] N. Eustathopoulos, *Metals* **2015**, *5*, 350.
50
51 [37] C. Garcia-Cordovilla, E. Louis, J. Narciso, *Acta Mater.* **1999**, *47*, 4461.
52
53 [38] X. Shen, M. Jing, W. Li, D. Li, *Powder Techn.* **2005**, *160*, 229.
54
55 [39] K. Nogi, N. Iwamoto, K. Ogino, *Transactions of JWRI* **1992**, *21*, 141.
56
57 [40] N. Eustathopoulos, B. Drevet, M. L. Muolo, *Mater. Sci. and Engin: A* **2001**, *300*, 34.
58
59 [41] B. R. Lawn, S. W. Freiman, T. L. Baker, D. D. Cobb, A. C. Gonzalez, *J. Am. Ceram. Soc.* **1984**,
60 *67*, c67.
61
62 [42] J. J. Kruzic, R. M. Cannon, R. O. Ritchie, *J. Am. Ceram. Soc.* **2005**, *88*, 2236.
63
64 [43] P. Chantikul, S. J. Bennison, B. R. Lawn, *J. Am. Ceram. Soc.* **1990**, *73*, 2419.
65
66 [44] R. G. Munro, *J. Am. Ceram. Soc.* **1997**, *80*, 1919.

- 1
2
3
4 [45] Z. A. Munir, U. Anselmi-Tamburini, M. Ohyanagi, *J. Mater. Sci.* **2006**, *41*, 763.
5
6 [46] R. Orrù, R. Licheri, A. M. Locci, A. Cincotti, G. Cao, *Mater. Sci. and Engin: R: Reports* **2009**,
7 63, 127.
8
9 [47] Z. Xu, J. Huang, C. Zhang, S. Daryadel, A. Behroozfar, B. McWilliams, B. Boesl, A.
10 Agarwal, M. Minary-Jolandan, *Adv. Engin. Mater.* **2018**, *20*, 1700782.
11
12 [48] H. L. Ferrand, F. Bouville, T. P. Niebel, A. R. Studart, *Nature Materials* **2015**, *14*, 1172.
13
14 [49] M. J. Garnier, D. C. Dunand, *Mater. Sci. and Engin: A* **2019**, *743*, 190.
15
16 [50] ASTM Standard D790 *Standard Test Methods for Flexural Properties of Unreinforced and*
17 *Reinforced Plastics and Electrical Insulating Materials*, ASTM International, **2017**.
18
19 [51] ASTM Standard E1820 *Standard Test Method for Measurement of Fracture Toughness*, ASTM
20 International, **2016**.
21
22
23
24
25
26
27
28
29
30
31
32
33
34
35
36
37
38
39
40
41
42
43
44
45
46
47
48
49
50
51
52
53
54
55
56
57
58
59
60
61
62
63
64
65



52 **Figure 1.** (A) Flow chart summarizes the “bottom-up” processing to create nacre-like (brick-and-
53 mortar) alumina structures. SEM micrographs illustrates the nature of the nickel-phase “mortar”
54 formed within Ni+NiO-coated alumina and Ni-coated alumina samples with 5 μm scale bars. In the
55 Ni+NiO-coated samples, sintering at (B) 1100°C generates a sheet of nickel that sits between the
56 alumina platelets, whereas sintering at (C) 1200°C causes the nickel to dewet and act as ball-shaped
57 impurities in the alumina. For the Ni-coated materials, nickel dewets at both sintering temperatures,
58 (D) 1100°C and (E) 1200°C. The blue lines are EDS line scan results to show changes in nickel content.

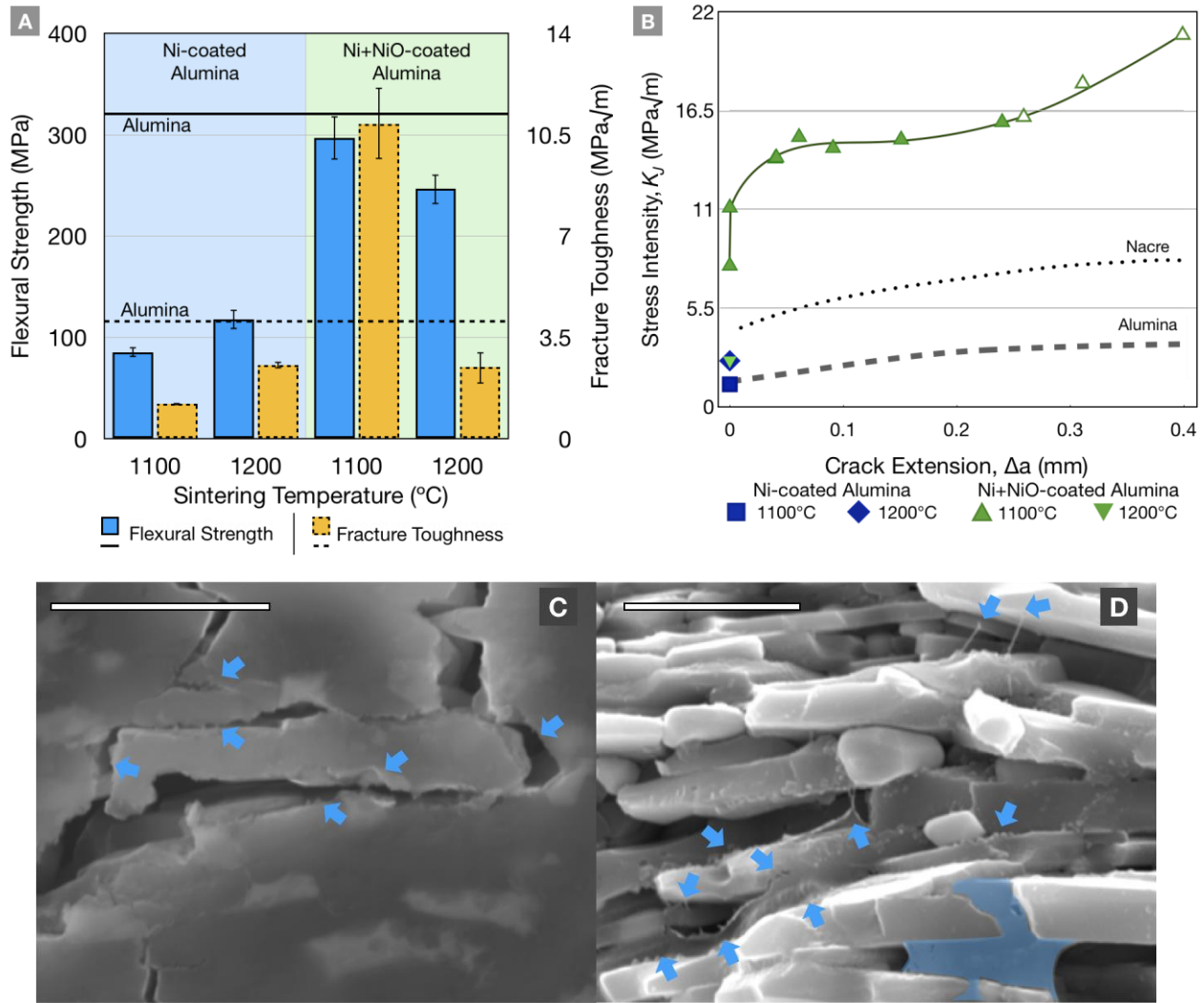


Figure 2. Summarized mechanical testing results in bar graphs, showing (A) flexural strength and fracture toughness test results. The Ni+NiO-coated samples sintered at 1100°C show (B) R-curve behavior that enhances the fracture toughness of the material from $\sim 8 \text{ MPa}\cdot\text{m}^{1/2}$ to $16 \text{ MPa}\cdot\text{m}^{1/2}$ associated with slow (stable) crack growth, toughness behavior that is far superior to that of fine-grained monolithic alumina (and even nacre). In contrast, the samples sintered at 1200°C or with only Ni-coated platelets display no R-curve behavior and fracture catastrophically with a fracture toughness lower than alumina. The unfilled points are data points that are not strictly “valid” according to ASTM Standard E1820 because they exceed the maximum crack extension for the size of the test specimens. SEM micrographs with 5 μm scale bars illustrate the salient toughening mechanisms in the Ni+NiO-coated alumina samples sintered at 1100°C. Although there is some Ni dewetting based on the brighter areas in (C), evidence of nickel tearing (highlighted by blue arrows) and ceramic “brick” pull-out are observed along crack path. The fracture surface in (D) shows more signs of nickel tearing in between the platelets, indicated by the blue arrows, with untorn nickel in the blue region. This suggests that the inter-brick displacements and the resulting fracture paths may occur *within* the nickel mortar phase rather than along the Al_2O_3 -ceramic/Ni-metal interfaces.

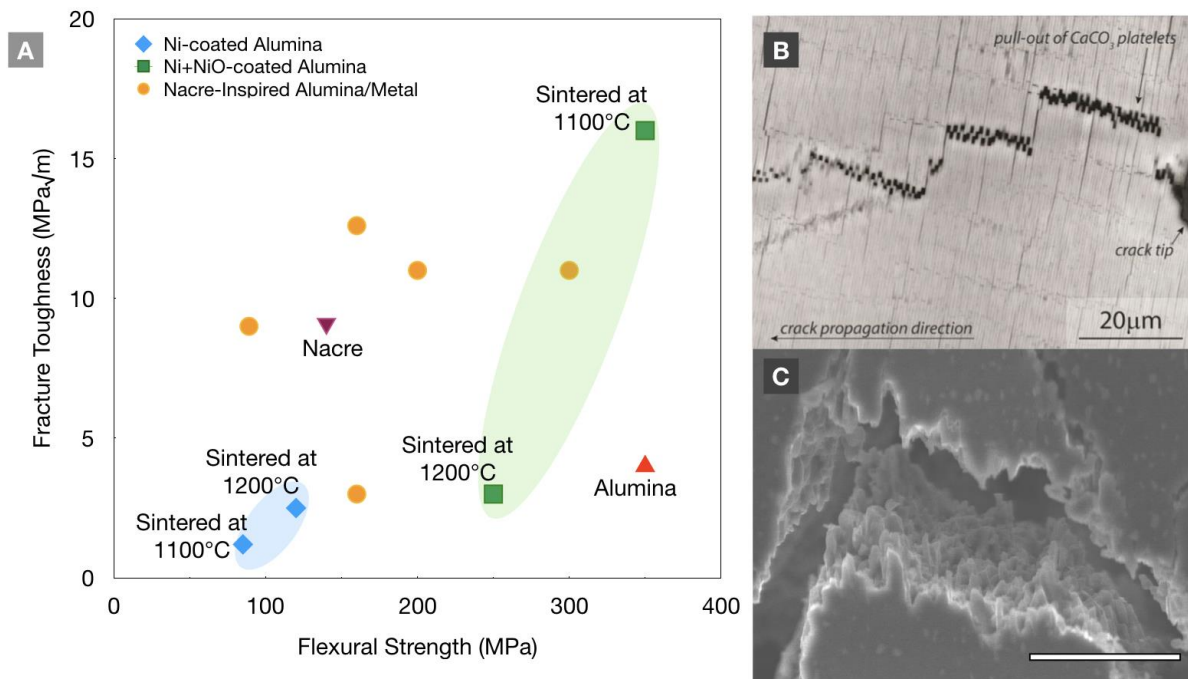


Figure 3. (A) Comparison of reported mechanical properties of bioinspired (nacre-like) alumina ceramics containing less than 10 vol.% metallic mortar, taken from refs. [23,24,29,47,48] (circular data points), with that of nacre (triangular data point) and the current results (square and diamond data points) to illustrate how the composition, processing, and sintering temperature can affect their damage-tolerance (strength and toughness). Scanning electron micrograph of the path of a crack in (B) natural nacre and (C) Ni+NiO-coated alumina sintered at 1100°C (with a 25 μm scale bar), shows toughening via the pull-out of the platelets (with displacements in the range of a few micrometers) leading to crack bridging, the coarser-scale deflection of the crack path, roughly perpendicular to orientation of the platelets, and the corresponding formation of a rough fracture surface as the crack tried to maintain a macroscopic path nominally perpendicular to the applied tensile stress. (image (B) courtesy of Bernd Gludovatz)

Supporting Information for

Bioinspired Nacre-like Alumina with a Metallic Nickel Compliant-Phase Fabricated by Spark-Plasma Sintering

Amy Wat^{1,2}, Claudio Ferraro³, Xu Deng⁴, Andrew Sweet², Antoni P. Tomsia¹,
Eduardo Saiz³ and Robert O. Ritchie^{1,2}

1. Materials Sciences Division, Lawrence Berkeley National Laboratory, Berkeley, CA 94720, USA

2. Department of Materials Science and Engineering, University of California, Berkeley, CA 94720, USA

3. Department of Materials, Imperial College London, London SW7 2AZ, UK

4. Center for Colloids and Smart Interface, University of Electronic Science and Technology of China, Chengdu 610054, China

Coating Technique

Before processing, the as-received alumina platelets were coated with a nickel shell using a coating procedure modified from Shen, *et al.*^[38], with a flow chart summarizing the processing of the core-shell platelets as shown in [Figure S1](#). The alumina platelets were suspended in deionized (DI) water with a concentration of 20g/L. The suspension was magnetically stirred and aqueous solutions of nickel sulfate heptahydrate (Sigma Aldrich, St. Louis, MO) and ammonium bicarbonate (Sigma Aldrich, St. Louis, MO), respectively with a molarity of 0.8M and 1.5M, were added into the suspension gradually to initiate the precipitation reaction. The solutions were maintained, with stirring, at 25°C for 12 hr. Subsequently, the platelets were washed and filtered four times with DI water, followed by drying in 60°C air for 12 hr. The dry platelets were calcinated at 600°C for 2 hr with a heating rate of 1°C/min in an air furnace (Thermolyne, Thermo Scientific, Waltham, MA) followed by 2 hr reduction in hydrogen at 600°C in a modified Abar 90 High Temperature Vacuum Furnace (Bensalem, PA).

Fracture Toughness and Strength Calculations

Due to the small size of the samples, in this study nonlinear-elastic fracture mechanics measurements were used to evaluate the fracture toughness in terms of J -based crack-resistance curves (R-curves). J refers to the J -integral, which is a field parameter that describes the local stress and displacement fields at the crack tip in a nonlinear-elastic solid. It is also the nonlinear-elastic

1
2
3
4 equivalent of the strain-energy release rate, specifically the rate of change in potential energy per
5 unit increase in crack area in a nonlinear-elastic solid. The R-curve shows plots of the value of J
6 necessary to enable stable crack growth. The crack extension was measured using the elastic
7 unloading compliance of the specimen. The corresponding J value for each crack extension was
8 found using the summation of its elastic and plastic components. The elastic component of J was
9 found using the linear-elastic stress intensity value since $J_{el} = K^2/E'$, where $E' = E$ (Young's
10 modulus) in plane stress and $E/(1 - \nu)^2$ in plane strain (ν is Poisson's ratio). The plastic component
11 was based on the plastic portion of the area under the load-displacement curve, A_{pl} . The
12 expression, $J_{pl} = 1.9A_{pl}/Bb$, shows a relationship between the plastic component of J , J_{pl} , with A_{pl} ,
13 and the uncracked ligament size, b , and the sample thickness, B . J values were converted into the
14 equivalent stress-intensity K values using the standard mode I J - K equivalence of $K = (J.E')^{1/2}$.
15 Further details are given in the ASTM Standard E1820² and a previous study³ for fracture
16 toughness measurements.
17
18
19
20
21
22
23
24
25
26
27
28
29

30 Details on flexural strength calculations can be found in the ASTM Standard D790⁴.
31
32
33

34 **Supplementary References**

- 35 1. Shen, X., Jing, M., Li, W. & Li, D. Fabrication of Fe-, Ni- and FeNi-coated Al₂O₃ core-shell
36 microspheres by heterogeneous precipitation. *Powder Technology* **160**, 229–233 (2005).
37
- 38 2. ASTM Standard E1820, 2016, Measurement of fracture toughness, American Society for
39 Testing and Materials International, West Conshohocken, PA, 2016, www.astm.org.
40
- 41 3. Munch, E., Launey M.E., Alsem, D.H., Saiz, E., Tomsia, A.P. & Ritchie R.O. Tough, bio-
42 inspired hybrid materials. *Science* **322**, 1516–20 (2008).
43
- 44 4. ASTM Standard D790, 2017, Test methods for flexural properties of unreinforced and
45 reinforced plastics and electrical insulating materials, American Society for Testing and
46 Materials International, West Conshohocken, PA, 2017, www.astm.org.
47
48
49
50
51
52
53
54
55
56
57
58
59
60
61
62
63
64
65

1
2
3
4
5
6
7
8
9
10
11
12
13
14
15
16
17
18
19
20
21
22
23
24
25
26
27
28
29
30
31
32
33
34
35
36
37
38
39
40
41
42
43
44
45
46
47
48
49
50
51
52
53
54
55
56
57
58
59
60
61
62
63
64
65

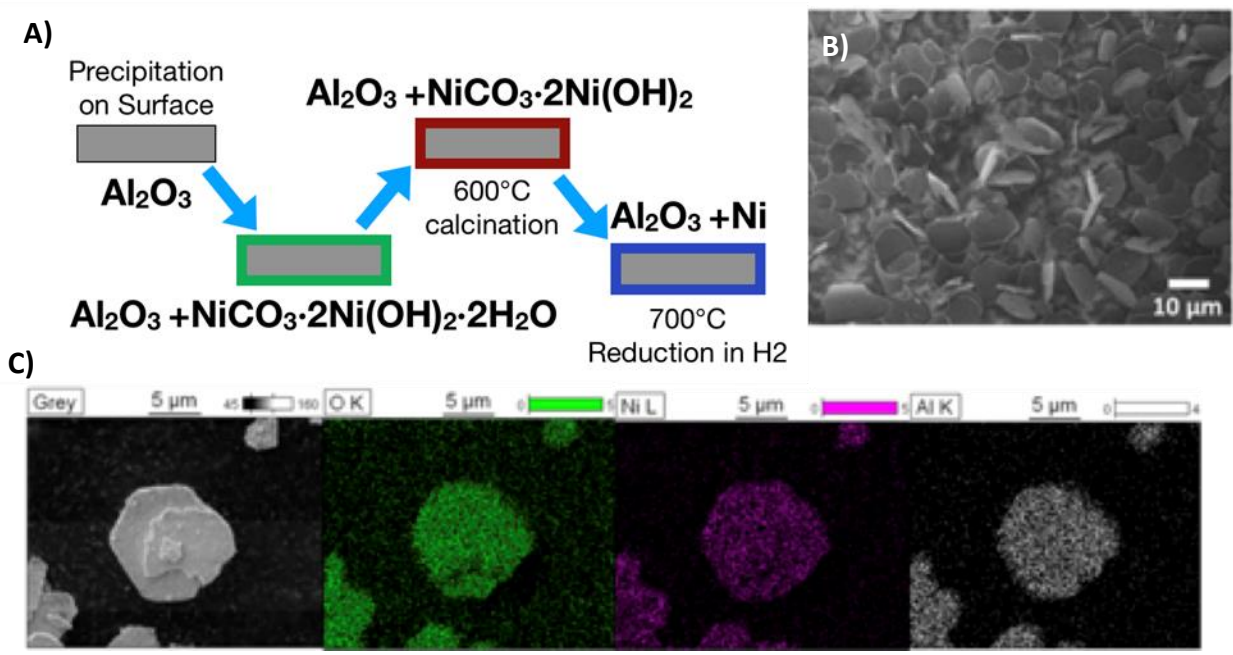


Figure S1. (A) Flow chart summarizing procedure used to coat the alumina platelets with nickel. (B) SEM micrograph of alumina platelets after coating. (C) EDS mapping of nickel coated alumina platelets that indicate how the platelets have been completely coated with nickel.

1
2
3
4
5
6
7
8
9
10
11
12
13
14
15
16
17
18
19
20
21
22
23
24
25
26
27
28
29
30
31
32
33
34
35
36
37
38
39
40
41
42
43
44
45
46
47
48
49
50
51
52
53
54
55
56
57
58
59
60
61
62
63
64
65

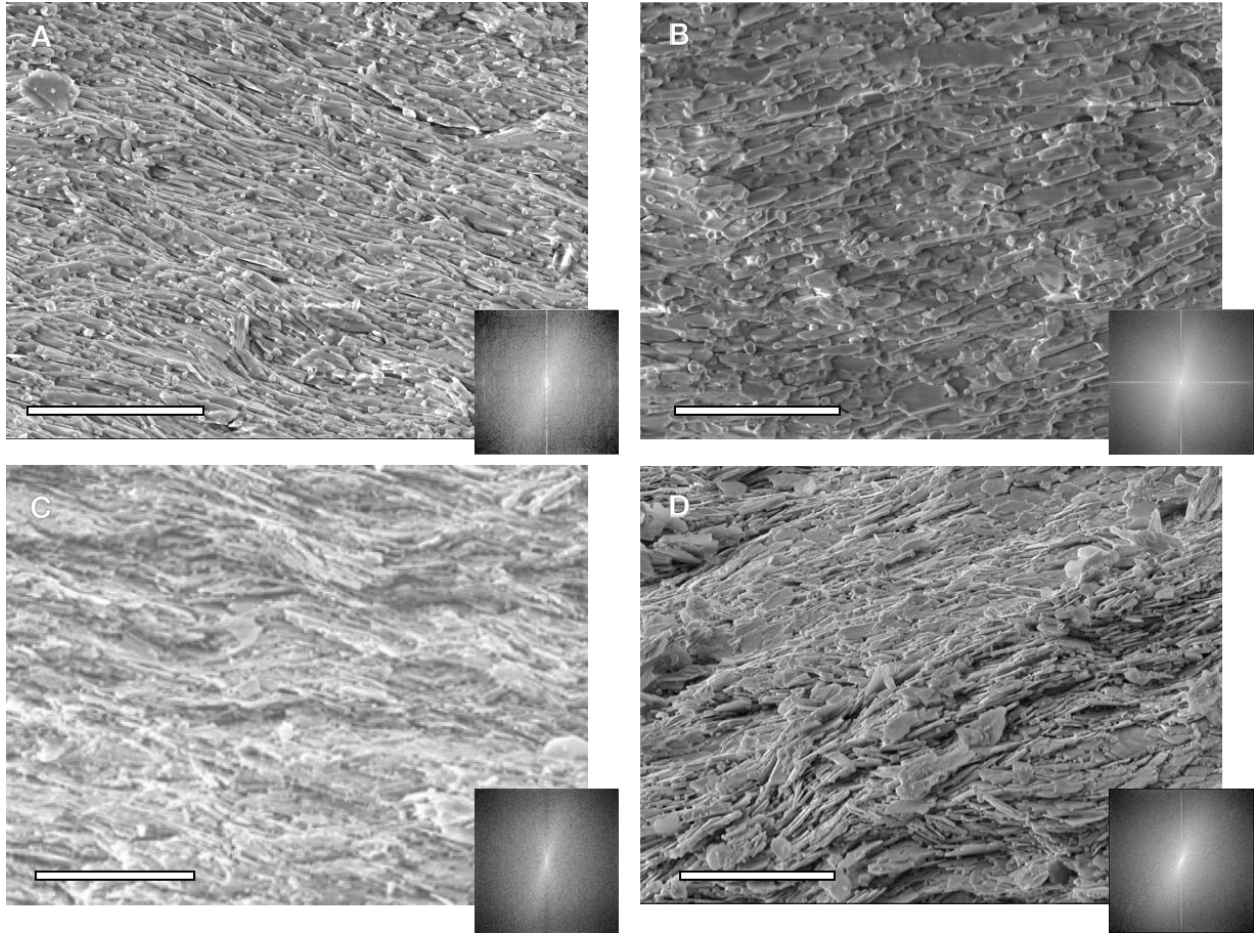


Figure S2. Scanning electron micrographs of the fracture surfaces of Ni+NiO-alumina samples sintered at 1100°C (A) and 1200°C (B) and Ni-alumina samples sintered at 1100°C (C) and 1200°C (D). The insets are fast Fourier transforms obtained from each SEM image. Based on the anisotropic nature of the fast Fourier transformed images, it is clear that samples were well aligned. It is particularly interesting to note how the basal planes are facing a uniform direction, avoiding any stacking card faults. All scale bars represent a length of 30 μm .

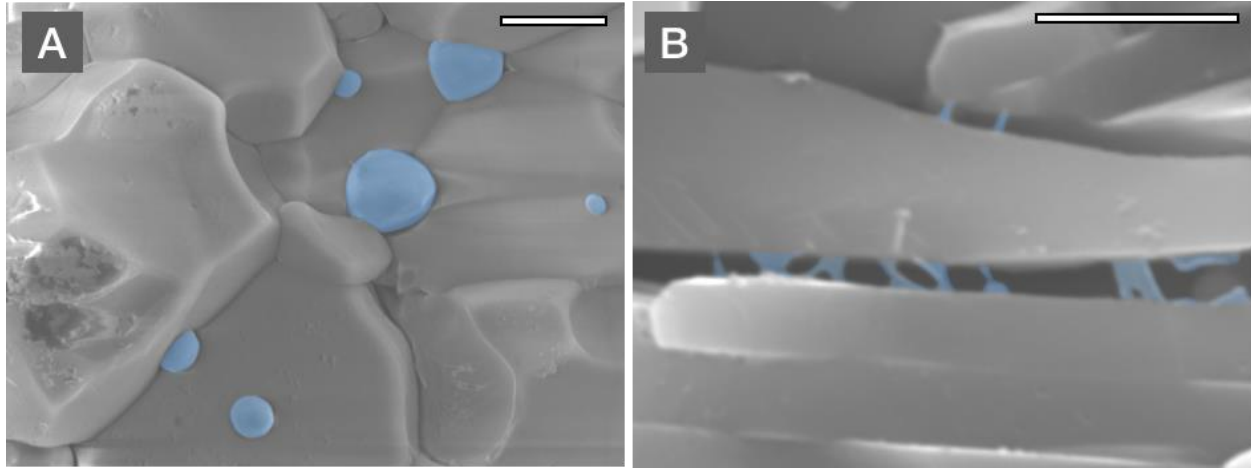


Figure S3. SEM micrographs illustrating the nature of the nickel-phase “mortar” formed within Ni+NiO-coated alumina samples. When sintered at (A) 1300°C, the Ni+NiO samples display further dewetting of the nickel and grain growth of the alumina. In the Ni+NiO samples, sintering at (B) 1100°C generates a sheet of nickel (highlighted blue) that sits between the alumina platelets with some discontinuities. The scale bars are 5 μm in figure (A) and 2 μm for figure (B).



Click here to access/download
Production Data
Abstract_awat.docx

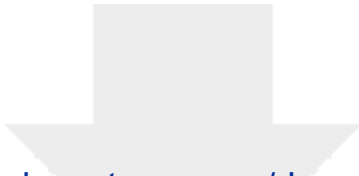




Click here to access/download

Production Data

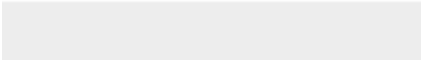
Bioinspired Nacre--SPS NAP-
final_SmallResponse1.docx



Click here to access/download

Production Data


Bioinspired Nacre--SPS NAP-SI.docx



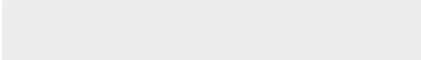



Click here to access/download
Production Data
Figure 1.jpg





Click here to access/download
Production Data
Figure 2.jpg

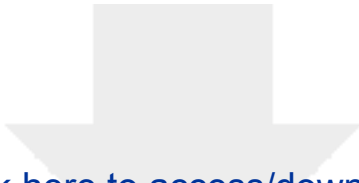




Click here to access/download

Production Data
Figure 3.jpeg





Click here to access/download

Production Data

[Nacre-SPS Graphical Abstract_awat.docx](#)

